

In-situ study of InAs quantum dots encapsulated in asymmetric (Al)GaAs confinement barriers

C. A. Mercado-Ornelas^a, L. I. Espinosa-Vega^a, I. E. Cortes-Mestizo^b, C. M. Yee-Rendón^c, E. Eugenio-López^{a,d}, J. P. Olvera-Enriquez^a, F. E. Perea-Parrales^a, A. Belio-Manzano^a, and V. H. Méndez-García^{a*}

^aCenter for the Innovation and Application of Science and Technology, Universidad Autónoma de San Luis Potosí, Av. Sierra Leona #550, Col. Lomas 2a Sección, 78210, San Luis Potosí, México.

^bCONACYT-Center for the Innovation and Application of Science and Technology, Universidad Autónoma de San Luis Potosí, Av. Sierra Leona #550, Col. Lomas 2a Sección, 78210, San Luis Potosí, México.

^cFacultad de Ciencias Físico-Matemáticas, Universidad Autónoma de Sinaloa, Av. de las Americas y Blvd. Universitarios, Cd. Universitaria, 8000 Culiacán Sinaloa, México

^dZentrum für Oberflächen-und Nanoanalytik Johannes Kepler University, Linz, Austria.

Received 8 October 2021; accepted 11 November 2021

In this work the self-assembling of InAs quantum dots (QDs) within asymmetric barriers of (Al)GaAs is studied via reflection high energy electron diffraction (RHEED). A comparative study between the AlGaAs/InAs/GaAs interfaces and its mirror-like heterostructure GaAs/InAs/AlGaAs showed significant differences in the self-assembling and capping of the QDs. The critical thickness of InAs QDs was proven to be larger when it is grown on AlGaAs alloys, compared with the deposition on GaAs layers. This change is explained by the reduced mobility of In atoms on the Al-containing surfaces, for which the QDs density is increased. Through the in-situ analysis of diffusion parameters, it is concluded that the mobility of In atoms decreases the mass transport of 2D and 3D precursors that conduces to the self-assembling of the QDs nanoislands, modifying the rate at which the QDs are formed. Further, during the first stages of QDs capping it is observed that the III-V materials intermixing plays a predominant role. The nanoislands are less affected when are covered by AlGaAs in comparison with the GaAs capping, preserving the QDs morphology and avoiding materials alloying. By following the RHEED intensity behavior during the QDs capping, a model was proposed to obtain quantitative parameters for the smoothing process. High-resolution x-ray diffraction (HRXRD) measurements show the composition of sharp interfaces for the AlGaAs/InAs/GaAs heterostructure. Lastly, numerical simulations were performed to evaluate the strain changes using the experimental information as input data.

Keywords: InAs-quantum dots, asymmetric quantum wells, intermixing, interfaces, strain.

DOI: <https://doi.org/10.31349/RevMexFis.68.031002>

1. Introduction

The development of semiconductor quantum dots (QDs) has been of great interest in the last decades because of their unique quantum confinement properties [1] such as the increased density of states and energy level discretization, which offers significant advantages when applied to electronic and optoelectronic devices [1-3]. Some current applications of QDs into devices are high-efficiency lasers, infrared detectors, storage appliances, light emitter diodes (LEDs) and solar cells. One of the most common methods to synthesize semiconductor QDs is by allowing for the self-assembling of nanoislands by the Stransky-Krastanov growth mode (SK). In this growth mode at the beginning of the deposition the adatoms nucleates two-dimensionally. The epilayer/substrate lattice mismatch conduces to the strain accumulation as the growth proceeds, until that for some thickness the elastic energy is no longer sustainable and the film relaxes forming 3D islands, termed as QDs if these are capable to achieve electron quantum confinement. The thickness at which the relaxation occurs is known as the critical thickness (H_c), and the film that stays 2D after the relaxation below the QDs and uniformly covering the substrate is known as the

wetting layer (WL). SK growth mode depends on strain and epilayer/substrate free energies and it is regularly employed with high precision deposition techniques such as molecular beam epitaxy (MBE) [4-5].

In addition, to take advantage of QDs properties in devices, it is necessary to explore mechanisms to successfully stack several QDs layers, which depend on many parameters such as confining or barrier layers, wetting layers, composition and morphology of the QDs, among others [6-7]. Nevertheless, as any process of encapsulation of strained materials, different effects such as intermixing, diffusion, segregation and the strain itself affect the islands geometry and therefore their crystal, structural, optical and optoelectronic properties [4,6,8].

The encapsulation process of InAs QDs with GaAs matrix has been commonly studied [2], [8]. However, InAs self-assembled quantum dots (SAQDs) embedded with different III-V semiconductors alloys as matrix layers, establishing asymmetric quantum wells (AQWs) layer are not fully explored. It is expected that complex heterostructures with SAQDs embedded in AQWs offer another design parameters that might lead to enhance their structural and optical properties, such as specific QDs sizes and distributions, increase

of the photo-generated carriers and stronger quantum confinement effects, which might lead to further applications of QDs photovoltaic devices [9,10].

Further, the asymmetric encapsulation in the multistacking of SAQDs modifies the strain effects and crystal quality from the AQWs interfaces, thus morphological and optical characteristics of the QDs are expected to be modified as well. The quantum confinement states or energy levels of QDs will depend on the asymmetry of the AQWs. The heterointerfaces in AQW change by the addition of QDs, the bands discontinuity between the QDs and their matrix layers, enhance the charge transfer and increase the charge mobility in the device [4,5,9]. Hence, it is expected that the implementation of QDs embedded AQWs will yield greater distribution of photogenerated carriers, and significant improvements in the efficiency of photovoltaic devices [10].

In this work, the authors describe and analyze the nucleation and capping processes of the QDs through reflection high energy electron diffraction (RHEED) and kinematical theory, with the main aim to estimate crucial differences in the QDs structural characteristics employing asymmetric (Al)GaAs matrix layers. High resolution x-ray diffraction (HRXRD) and numerical simulations were employed to sustain the experimental assumptions determined by RHEED.

2. Materials and methods

The samples were grown on epi-ready GaAs (100) Si doped substrates in a Riber-32 MBE system equipped with an *in situ* RHEED characterization technique. First, the substrates native oxides were desorbed at 580°C, and then a 350 nm thick silicon doped GaAs buffer layer was deposited. Afterward, asymmetric quantum wells growth was performed in two heterostructures. For the first one (AQW1), the QDs were grown on GaAs and later capped with Al_{0.3}Ga_{0.7}As. The sequence of layers Al_{0.3}Ga_{0.7}As/InAs/GaAs (30 nm/2.7 ML/7 nm) was repeated five times. Each of this sequence of layers is termed asymmetric quantum well (AQW1) since the height of potential barrier for InAs is different below and above it. For the second sample (AQW2) the QDs were grown on Al_{0.3}Ga_{0.7}As and later were capped with GaAs according to the sequence of layers GaAs/InAs/Al_{0.3}Ga_{0.7}As (30 nm/2.5 ML/7 nm). The sequence of these layers was also repeated five times. The Al concentration in AlGaAs alloys was 30%. Prior to the growth of the InAs QDs the substrate temperature was decreased to 480°C for all the five periods, where the surface exhibited the C(4 × 4) surface reconstruction. For the capping of the QDs, either with GaAs or AlGaAs, the first 10 nm were grown at 480°C to avoid In evaporation and then the substrate was rapidly increased up to 580°C to grow an additional layer of 20 nm. The (2 × 4) surface reconstruction was observed in this step. After the growth of the five periods, the heterostructures were capped with a 100 nm-thick intrinsic GaAs layer followed of 200 nm of Be doped GaAs. A scheme of the heterostructures is appreciated in Fig. 1. The self-assembling process was monitored along the [011]

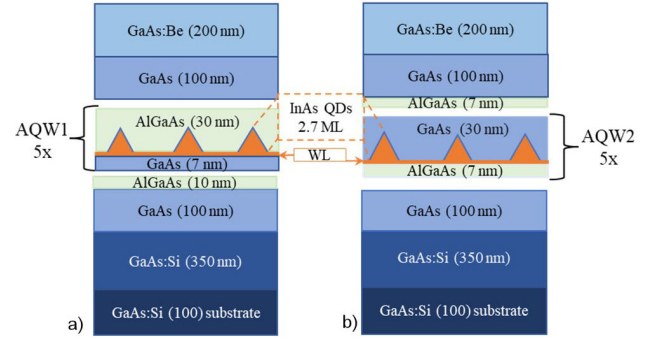


FIGURE 1. Sketch of the studied AQW samples a) Al_{0.3}Ga_{0.7}As/InAs/GaAs (AQW1) and b) GaAs/InAs/Al_{0.3}Ga_{0.7}As (AQW2).

azimuth to confirm the 2D - 3D transition with the typical chevron-like spots.

(HRXRD) measurements were done using a Panalytical Empyrean diffractometer with a Cu- K_{α} wavelength (1.5406 Å), the scans were performed on the diffraction angle ($\omega - 2\theta$) rocking curves. Further, two-dimensional (2D) numerical simulations were performed using the finite element method to investigate the strain fields propagation. The model implemented was the strain minimization model of the total elastic energy through a conjugate gradient method, which it is used to find the equilibrium positions of the atoms in the lattice structure, this approach allows us to obtain the local strain tensor in the QDs heterostructures [11]. The experimental characterization was employed to provide input data for the geometrical aspects in the samples.

3. Results and discussion

RHEED has been used to track the QDs formation from the 2D to 3D transition, and during the capping procedure. Figure 2 shows the (002) RHEED spot intensity taken during the first AQW for both heterostructures and along the [011] azimuth as a function of the InAs thickness growth. Some evident differences can be perceived close to the 2D-3D growth mode transition depending if the InAs is grown either on GaAs (AQW1) or AlGaAs (AQW2). For instance, H_c and the slope of the intensity curve close to the 2D-3D transition resulted larger for the growth on AlGaAs in comparison to the growth on GaAs. The continuous lines in Fig. 2 are fits of equation

$$I(t) = \Delta I \left(1 - e^{-\gamma(t-H_c)} \right), \quad (1)$$

where γ is a rate constant and H_c is the InAs/(Al)GaAs critical thickness [12]. This equation matches satisfactorily the region close to the 2D-3D transition, which carries out most of the information concerning to the QDs nucleation process. The variation of H_c and γ with the number of AQW is plotted as inset in Fig. 2. It shows that independent of the number of AQW, H_c is smaller for AQW1 than for AQW2. In other words, the InAs islands tend to be nucleated slightly sooner

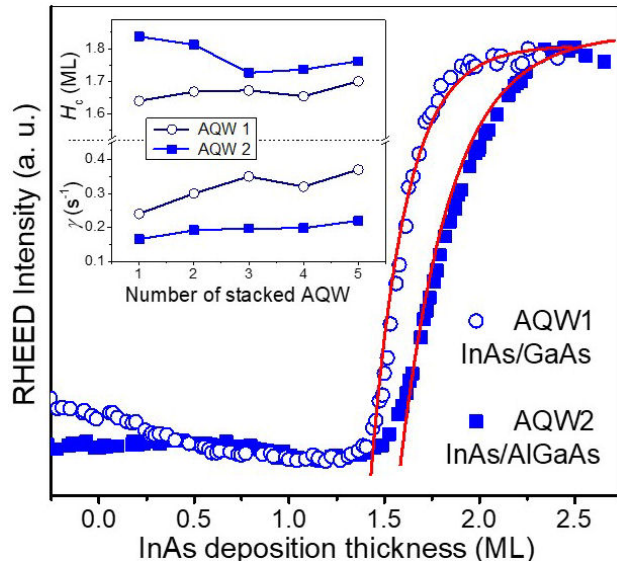


FIGURE 2. RHEED intensity curves taken for the first period of the InAs QDs grown on GaAs for AQW1 (open symbols) and on AlGaAs for AQW2 (solid symbols). The continuous lines correspond to fittings in the 2D-3D transition region of $I(t)$, the Eugenio-Song equation [12]. The insets show the behavior of H_c and γ with the number of AQW deposited in the heterostructure.

on GaAs than on AlGaAs, which could mean that the thickness of the WL is thinner when the InAs growth proceeds on GaAs.

The augmentation of H_c with the Al concentration in the surface material over which the InAs is grown, has been previously reported in literature [7,13] and it can be considered as one of the utmost significant results in epitaxial self-assembling of semiconductor nanostructures. Since the epilayer/substrate lattice mismatch does not vary with the Al mole fraction this experimental result is evidence that the self-assembling phenomena of QDs is a subtle assistance between kinetic adatoms diffusion mechanisms and thermodynamic strain relaxation to reach an equilibrium condition. Concerning to strain it is understood that the 2D-3D growth mode transition in lattice mismatched systems such as InAs/(Al)GaAs takes place after growing an epilayer of thickness after which no more elastic energy can be stored, and the relaxation occurs via the self-assembling of nanoislands. Nevertheless, the InAs/(Al)GaAs misfit strain is quite similar for AQW1 and AQW2, 6.685 and 6.646, respectively and yet H_c experiences significant variations. Thus, the surface diffusion properties are responsible to mark the differences in H_c . The delay of the InAs 2D-3D transition can be explained by deficiencies of material motion on the surface associated to the reduced In adatoms mobility on Al containing surfaces with respect to GaAs surfaces [13,14].

An increased H_c is equivalent to build a thicker WL, which results on the formation of 2D and 3D adatoms precursors as explained in the following lines. The mean-field theory employed to describe the QDs island nucleation by the Stransky-Krastanov growth mode developed by Doobs et al. [15] considers the movement of adatoms on the surface and

the formation of 2D platelets and quasi-3D islands. The 3D islands may act as precursors providing atoms from their peripheral at the rate γ , and the migration to its top gives rise to the formation of a QD on the top of the WL. The 2D platelets are of utmost importance for the strain distribution during the growth and for the QDs vertical coupling during bilayers stacking [16]. The reduced mobility of In may conduce to the formation of high density yet small precursors. Since the mechanism of elastic deformation on top of the islands relieves strain the large density of 2D platelets obtained on AlGaAs surfaces increases the effectiveness to reduce strain during the InAs deposition, leading to the delay of the 2D-3D transition or equivalently to an increase of the WL thickness, and therefore the reduction in size of the QDs [6,7,17].

Further information can be obtained from Fig. 2. As explained previously the slope of the intensity curves changes for the growth of QDs on GaAs and AlGaAs surfaces. This region gives information of the rate of nucleation of islands mostly associated to the mass transport of 2D and 3D precursors that conduces to the self-assembling of the QDs nanoislands. The nucleation rate has been also associated to the rate γ of 2D precursors dissociation [17,18], which during the 2D-3D transition contributes significantly to the 3D self-assembling. The inset of Fig. 2 shows that the rate γ of AQW1 (growth on GaAs) is higher than that of AQW2 (growth on AlGaAs) indicating that the 3D self-assembling is slower for AQW2 due to the reduced mobility of In atoms on the Al-rich surface. The connection between the rate of 2D-3D nucleation and density of QDs has been corroborated for uncapped samples prepared under similar growth conditions and has been also documented in literature [12,19]. Additionally, note that in the sample AQW2, γ does not vary significantly with the number of AQWs, which is associated to few changes in size and distribution of QDs for consecutive layers as it is usual in vertically stacked layers [20,21].

In order to construct the AQW, the QDs of samples AQW1 and AQW2 were capped with an alloy material different than that used in the former InAs growth. The temporal evolution of the RHEED intensity of the (002)-diffraction spot along the $[0\bar{1}1]$ azimuth during the capping process of the InAs QDs with GaAs and AlGaAs for the first and fifth AQW are shown in Fig. 3a) and b), respectively. At the beginning of the (Al)GaAs deposition the intensity of the diffraction spots diminishes since smooth surfaces are gradually recovered. Still, the intensity curves show differences when covering with GaAs or AlGaAs. For instance, the capping with AlGaAs shows a quick intensity drop and nearly the same line-shape independent of the number of AQW layer. On the contrary, for the GaAs growth on InAs QDs the (002)-diffraction spot intensity initially shows a slight depreciation followed of a quick drop, and then the intensity is partially recovered. Therefore, for GaAs capping three regions were identified and labeled in Fig. 3a). Along with changes in intensity the RHEED screen showed the usual patterns observed for InAs covering, *i.e.* disappearance of the chevrons, dim-diffuse, and streaky pattern recovery. During the AlGas

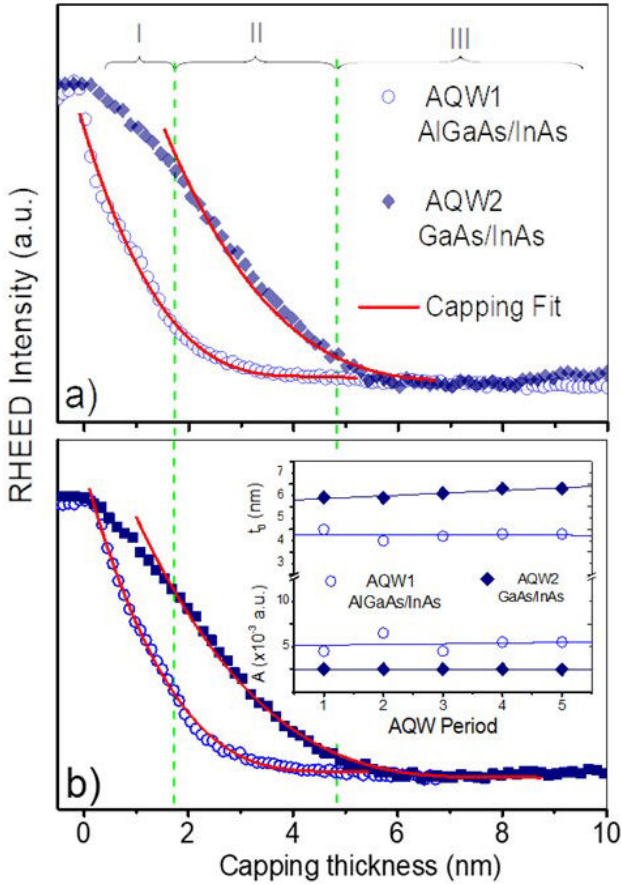


FIGURE 3. RHEED intensity curves recorded during the InAs QDs capping for the (a) first and (b) fifth AQW period. The experimental data are plotted with open and solid symbols for AQW1 and AQW2, respectively. The fittings of equations described in the text are indicated with continuous curves. The inset depicts the results for the coefficient diffusion (K_l) in the samples and the roughness coefficient (σ) for the capping layers.

capping a steady loss of the chevron like spot is observed as the thickness of the AlGaAs is increased suggesting gradual change in the QDs shape and surface roughness. Conversely, for the GaAs capping the chevrons rapidly change in angle and interestingly they last almost the same amount of time as the Region I does. The thickness of Region I is comparable with the thickness along which the InAs islands suffer most of the changes when capped with GaAs [22]. As it is known, during the early stages of capping, and besides of the surface capture of adatoms becoming from the impinging flux, additional dynamics processes occur like In-diffusing from the top of the QDs to the WL and In-Ga intermixing [22-24], this result in a sudden reduction in height and an increase of lateral dimensions. Therefore, the behavior of the spot intensity of Fig. 3 at the early stages of the capping overgrowth, is in complete agreement with the reported flattening and shape changes of InAs QDs for GaAs capping [23-24].

Another interesting subject is the thickness relation of Region I with the number of AQWs. For GaAs capping, Region I is close to 2.5 nm for the first 3 AQW layers, and then it

drops close to zero at the fifth AQW layer. On the contrary, for AlGaAs capping the Region I thickness is very close to zero for every AQW layer, and then nearly the same line-shape of the RHEED intensity is observed independent of the number of the stacked AQW period. These observations reinforce the idea that Region I is related with the interaction of the capping material with the InAs QDs apex; if the height of the islands is reduced with the number of AQW, then it drives through to a less sharply geometry and consequently a diminished interaction with In is expected. In other words, it is well documented for GaAs capping that as the number of QDs layers increases during vertical stacking the islands changes in size, usually decreasing in height and increasing in diameter [17,21,24-26]. These effects become more noticeable for the first stacked bilayers of QDs [17]. Therefore, since the first In atoms that interact with the capping materials become from the apex, when capped with GaAs, flatter islands would suffer minor changes during overgrowth, which explains the reduction in thickness of Region I as observed in Fig. 3. Conversely, as mentioned before the capping with AlGaAs showed a quick intensity drop independent of the number of AQW layer, in accordance with the considerable reduction of the InAs QDs flattening during the AlGaAs capping process, due to the reduced In migration from the apex towards the base of QDs.

In Region II the mass transport occurs to smooth the surface during the low temperature capping of islands either with GaAs or AlGaAs. Region I from AQW1 is very narrow, so for AlGaAs capping the Region II starts at cap-thickness close to zero. The intensity of the RHEED diffraction spots during the 3D-2D growth transition changes proportionally to the volume V_s of 3D features on the surface. Under the assumptions that the density of QDs stays constant along the capping process and that the arriving material is nucleated 2D uniformly from the base to apex, V_s would be solely related to the bare peak of the island as the covering proceeds. For instance, for pyramidal shaped islands the volume changes with the height of the deposited material as $V_s(y) = (A_b/h^2)(h-y)^3$ for an island of base A_b and height h . y is the grown thickness prior the whole capping, *i.e.*, $0 < y < h$. Therefore, the RHEED intensity curves from Region II were fitted to equation:

$$I(t) = I_0 + \tau [t_s - t]^3, \quad (2)$$

where, t is the cap thickness, I_0 is the background intensity of Region II curves, t_s is the thickness required to reach a smooth surface, τ is a fitting constant related with the rate at which the 3D nature of the surface is lost and is linked to the volume to be covered (*i.e.* size and density of nanoislands) and with the impinging flux, the adatoms sticking coefficient and diffusion parameters. Satisfactory fittings were obtained to the experimental data in Region II, as observed in Fig. 3. τ and t_s are plotted as a function of the number of AQW layers in the inset of Fig. 3 where is observed that the rate τ for GaAs is larger than for AlGaAs capping, while t_s follows the opposite trend. If the rate of covering islands is low, it would take longer time to get a smooth surface. In addition,

both values τ and t_s are almost the same for all the stacked AQWs, indicating good pairing between QDs layers, since these results suggest that the island distribution and geometry are nearly the same for each of the AQW layer.

The different values of t_s observed in the inset of Fig. 3 indicates that the flatness of the surface is recovered at different capping thicknesses, which is associated to both, the size of QDs prior to capping, and the consequent changes of QDs morphology provoked by the capping itself. Larger dots are synthesized for the growth of InAs on GaAs as compared with the growth on AlGaAs as observed by atomic force microscopy (AFM) for removed samples, and supported from Fig. 2 the *in situ* observation of H_c reduction [7,24,27]. During the capping process, GaAs strongly interacts with the InAs/AlGaAs structure conducting to roughening as compared with the ternary alloy capping. Therefore, this process makes more difficult to smooth a GaAs capped surface, in accordance with the larger t_s for AQW1. The low temperature capping process is very important to quench or reduce the QDs shape changes and materials intermixing, so the monitoring of the capping process can be very valuable to determine the precise thickness that will propitiate a proper covering, without sacrificing the QDs optoelectronic properties.

Close to 6 nm the RHEED intensity curves reach a minimum, thickness at which the islands are close to be fully covered either with AlGaAs (AQW1) or GaAs (AQW2), and hereafter the Region III is defined. In Fig. 3 is observed that the RHEED intensity in Region III is found to slightly increase with the layer thickness, associated to differences in surface mobility of adatoms at this temperature. Although it is worth to comment that at the end of the QDs capping carried out at high temperature streaky (2×4) RHEED patterns were observed for both AQWs samples, indicative that smooth surfaces were recovered. Thus, all the layers of QDs occurred on the same degree of flatness either on GaAs or AlGaAs surfaces. Therefore, the major differences among the heterostructures occurred during the InAs growth and during the initial stages of capping (Regions I and II).

The changes in adatom mobility, interaction cap-QDs, roughening, etc., can introduce differences between the AlGaAs/InAs and InAs/AlGaAs heterostructures in the crystal quality and strain distribution. Figure 4 shows X-ray rocking curves for both samples, recording the symmetric scan around the GaAs (004) Bragg reflection. The most intense peak in Fig. 4 located at 0° corresponds to the GaAs substrate, while at lower Bragg angles interference effects from the multilayered heterostructure displayed by satellites peaks are clearly appreciated. The diffraction curve of AQW1 displays nice and spatially ordered satellite peaks indicating that the active region of the AQWs interfaces has low defects suggesting a fully strained state [29-30]. Each one of the peaks represents the interface (AlGaAs/InAs) and their respective order of the period, starting from the zero-order (L) and successively to L_{-3} , whose total corresponds to the thickness of five periods. The AQW1 diffraction scan indicates a good pe-

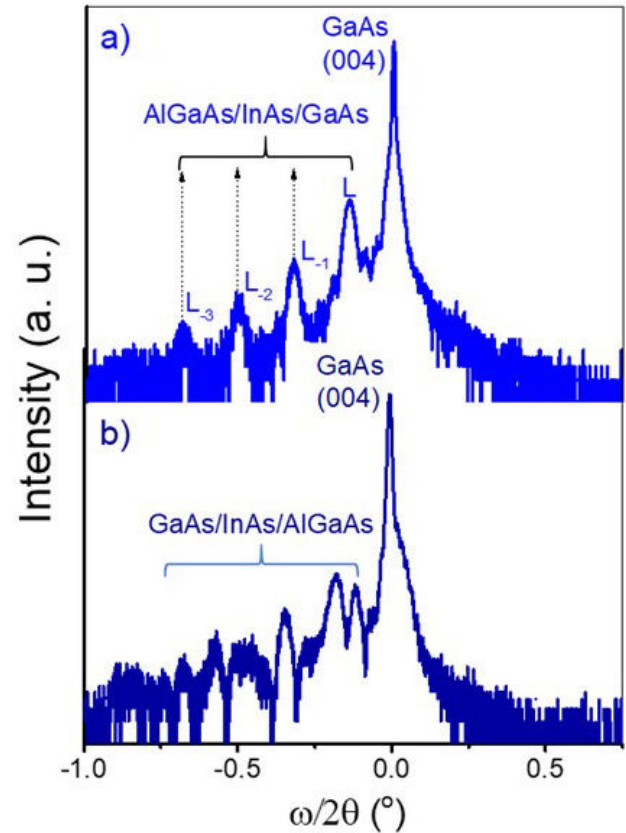


FIGURE 4. The $\omega - 2\theta$ experimental X-ray diffraction rocking-curves for a) AQW1 AlGaAs/InAs/GaAs heterostructure and b) AQW2 GaAs/InAs/AlGaAs sample.

riodicity and consequently a well-defined interface between the QDs and their capping layers. On the contrary, for the AQW2 sample decoupled satellite peaks formation is noticed, which provides information of diminished abruptness of interfaces either because the generation of defects resulted from partially relaxed interfaces [30-31], or by interdiffusion or intermixing within the periodic heterostructure [31]. The latter is quite plausible, as explained for AQW2 In atoms diffusion and In-Ga intermixing occurs changing the QDs morphology, inducing the InGaAs alloying regions effects [32], altering the crystallinity condition at the interface [33-35]. On the contrary, for AQW1 the Al adatoms bonds to In and reduce the In migration, this allows the QDs to preserve their morphology, and result in improvement of the QDs homogeneity and better interfaces formation [24,36]. Therefore, HRXRD verifies a better stacking and morphology of QDs for AQW1.

Furthermore, the average strain related with the modifications in the QDs morphology can be estimated from Fig. 4 through the following equation [30]

$$\varepsilon = \left[\frac{\sin(\Theta_{\text{GaAs}})}{\sin(\Theta_{\text{GaAs}} + \Delta\Theta)} \right] - 1, \quad (3)$$

where, $\Delta\Theta$ is angle separation from the GaAs substrate and the zeroth order peak. Strain values 0.0039 and 0.002 were obtained for samples AQW1 and AQW2, respectively.

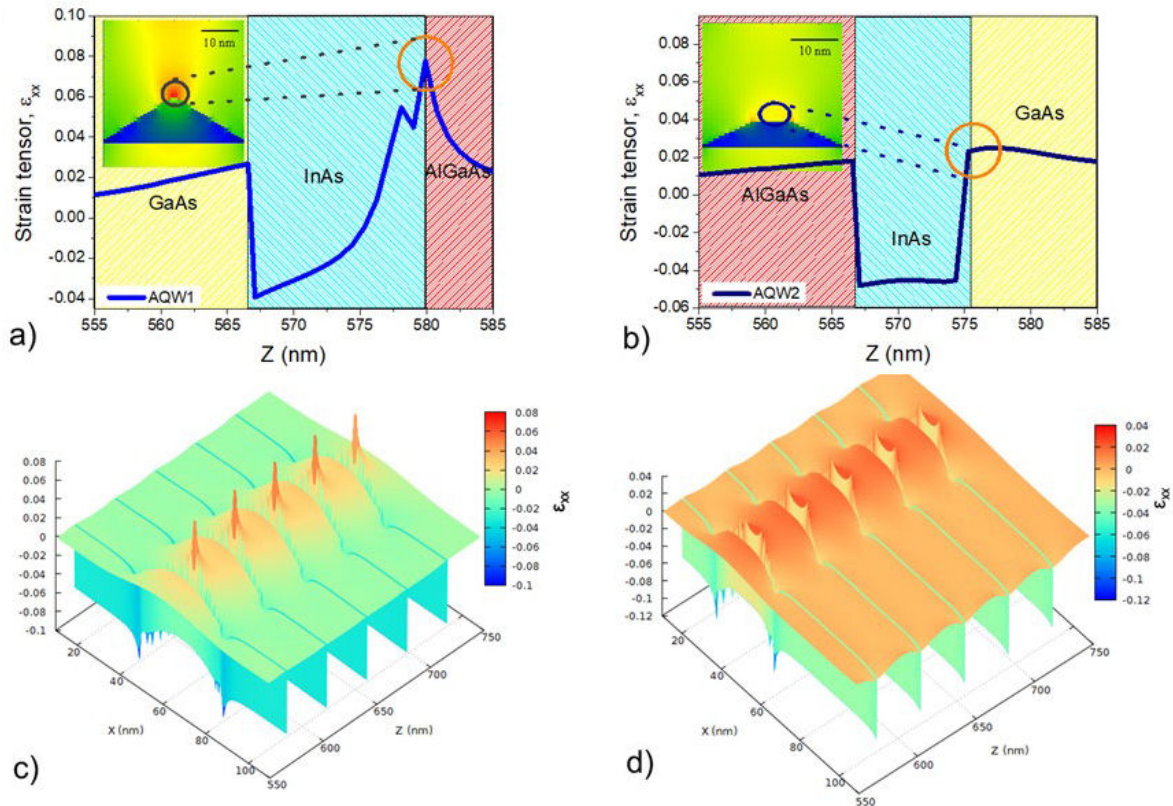


FIGURE 5. ϵ_{xx} profiles taken from strain simulations along the center of the QDs from the first AQW layer in a) AQW1 and b) AQW2. The insets show the QDs sketches for the 2D strain simulation for AQW1 and AQW2 with their respective QDs geometrical representation. The circle highlights the region of maximum strain ϵ_{xx} for AQW. 3D simulations of ϵ_{xx} for c) AQW1 and d) AQW2.

Hence, lower value of ϵ for sample AQW2 as compared with AQW1 indicates reduction of compressive strain.

Numerical simulations were employed to evaluate the variations of strain linked to changes in InAs-QDs morphology, which were sketched considering the changes depicted from RHEED observations and AFM. Pyramidal shapes were drawn for the QDs of AQW1 while truncated pyramids were sketched for AQW2 as it shown in Fig. 5, to the former a 40% reduction in height [26,37] and increase of QDs density (1×10^{10} to 1.4×10^{10} QDs/cm²) [7,19] were considered. Five periods of AQWs were vertically stacked for both simulated heterostructures. In order to account for the variation of the critical thickness observed by RHEED. The WL thickness for AQW2 was decreased from 0.52 to 0.50 nm from the first to the third period of the InAs QDs, since WL affects the strain distribution of InAs/(Al)GaAs self-assembled QDs.

The strain distribution for AQW1 and AQW2 are shown in Fig. 5a) and b) respectively, the ϵ_{xx} profiles were taken along the [1 0 0] direction and traced across the apex of the QDs for the first AQW layers and for two spacer layer thickness, 15 and 30 nm. The behavior of the strain distribution in the QDs for both heterostructures are alike independently of the spacer layer, *e.g.* tensile strain spread from the top and bottom of the nanoislands toward their capping layers, marked by the red and yellow region in the strain profiles of Fig. 5, while in the inside of the QDs compressive strain

highlighted by the blue region in the strain profile is appreciated. One of the parameters that determines the strain distribution is the spacer thickness [11,17,38-39]. The variation in the spacer layer thickness from 15 to 30 nm resulted very small difference, around 0.002 on the maximum value of strain with each other. Thus, the main changes of ϵ_{xx} are due to variations on the island shape related to the changes of WL and H_c . For 30 nm of spacer (close to the grown samples) $\epsilon_{xx} = 0.078$ at the center of the island and $\epsilon_{xx} = 0.02$ for AQW2. The simulated results clearly support the experimental results obtained by HRXRD, which sustains that the changes in QDs shapes reduces strain of AQW1 in comparison with AQW2.

Figure 5c) and d) shows 3D simulated strain profiles of the samples with a spacer layer thickness of 30 nm for AQW1 and AQW2 respectively. AQW1 revealed a top value of $\epsilon_{xx} = 0.078$ and is observed that the shape for QDs propitiates the spread of strain from the top of the nanoislands towards the subsequent stacked upper layer, enhancing the pairing probability of vertical stacking. Contrarily, for AQW2 truncated pyramids the maximum value is $\epsilon_{xx} = 0.04$. Thus, this particular shape of QDs leads the strain values on the surface of their capping layers, not very high or centered above the QD, and the strain distribution results to be more homogeneous at the interfaces, as a consequence the pairing probability is reduced for these regions and the nucleation centers

are harder to achieve. Hence, the variation of strain through the changes of the QDs morphology may conduce to having sharper interfaces, for instance the strain reduction and its distribution uniformity would drive to less sharp interfaces.

4. Conclusions.

To successfully achieve AQWs experimentally the quality of the interfaces must be precisely controlled not only to get closer to the theoretical design, but also because these frontiers have important consequences in the confinement properties of carriers. It is shown here that besides of carefully select appropriated growth parameters, the *in situ* characterization techniques can be exploited to control and eventually to tailor the deposition to improve the quality of multilayered QDs heterostructures. The delayed 2D to 3D growth mode transition of InAs on AlGaAs surfaces produces smaller QDs as compared with the growth on GaAs layers, but with advantageous on the QDs density. The drawback concerning the small QDs size can be overcome increasing the amount of deposited InAs. The intermixing in these strained systems

affect the QDs size and the layers interface abruptness, which undoubtedly conduce to the detriment of the crystal quality and optoelectronic properties of the heterostructures. The implementation of Al containing alloys would reduce these problems. The introduction of Al in any of the layers increase the potential barrier for the QDs propitiating advantageous confinement of carriers. Certainly, for thicker and higher Al concentration in AlGaAs compounds, the carriers would get trapped, which is not convenient for some applications. This study is expected to contribute to the understanding InAs QDs interfaces and further application in optoelectronic devices.

Acknowledgments

The authors acknowledge the financial support of FRC-UASLP and CONACYT-Mexico and Catedras CONACYT. CIACYT authors express their gratitude to Laboratorio Nacional de Analisis Fisicos, Quimicos y Biologicos de la UASLP.

1. H. Unlu and N.J.M. Horing (eds.). Low Dimensional Semiconductor Structures. NanoScience and Technology, Chapter 1, Springer, (2013). <https://doi.org/10.1007/978-3-642-28424-3>.
2. L. Peng, L. Hu and X. Fang. Low-Dimensional Nanostructure Ultraviolet Photodetectors. *Adv. Mater.* **25** 5321 (2013). <https://doi.org/10.1002/adma.201301802>.
3. A. D. Yoffe. Semiconductor quantum dots and related systems: Electronic, optical, luminescence and related properties of low dimensional systems. *Advances in Physics*, **50** **1** (2001) 1, <https://doi.org/10.1080/00018730010006608>.
4. K. Barnham and D. Vvedensky (eds.). Low-dimensional semiconductor structures: fundamentals and device applications. Cambridge University Press, (2001). <https://doi.org/10.1017/CBO9780511624247>.
5. J. Wu, S. Chen, A. Seeds and H. Liu. Quantum dot optoelectronic devices: lasers, photodetectors and solar cells. *J. Phys. D: Appl. Phys.* **48** (2015) 363001, <http://dx.doi.org/10.1088/0022-3727/48/36/363001>.
6. I. A. Karpovich *et al.*, Tuning the energy spectrum of InAs/GaAs quantum dots by varying the thickness and composition of the thin double GaAs/InGaAs cladding layer. *Semiconductors*, **38**, **4** (2004) 431, <https://doi.org/10.1134/1.1734670>.
7. M.V. Rakhlin *et al.*, InAs/AlGaAs quantum dots for single-photon emission in a red spectral range. *Sci. Rep.* **8** (2018) 5299, <https://doi.org/10.1038/s41598-018-23687-7>.
8. P. Werner, K. Scheerschmidt, N. D. Zakharov, R. Hillebrand, M. Grundmann and R. Schneider, Quantum Dot Structures in the InGaAs System Investigated by TEM Techniques. *Cryst. Res. Technol.* **75** (2000) 9, [https://doi.org/10.1002/1521-4079\(200007\)35:67759::AID-CRAT7593.0.CO;2-W](https://doi.org/10.1002/1521-4079(200007)35:67759::AID-CRAT7593.0.CO;2-W).
9. G. Yusa and H. Sakaki. Trapping of photogenerated carriers by InAs quantum dots and persistent photoconductivity in novel GaAs/n-AlGaAs field-effect transistor structures. *Appl. Phys. Lett.* **70** (1997) 345, <https://doi.org/10.1063/1.119068>.
10. A. Sayari, M. Ezzidini, B. Azeza, S. Rekaya, E. Shalaan, S.J. Yagmour, A.A. Al-Ghamdi, L. Sfaxi, R. Mghaieth, H. Maaref. Improvement of performance of GaAs solar cells by inserting self-organized InAs/InGaAs quantum dot superlattices. *Solar Energy Materials and Solar Cells*, **113** (2013) 0927, <https://doi.org/10.1016/j.solmat.2013.01.033>.
11. S. Birner *et al.*, Modeling of Semiconductor Nanostructures with nextnano. *Acta Physica Polonica. A.* **110** (2006) 2, <http://doi.org/10.12693/APhysPolA.110.111>.
12. E. Eugenio-Lopez *et al.*, InAs quantum dots nucleation on (100) and anisotropic (631)-oriented GaAs substrates. *Physica E* **95** (2018) 22, <http://dx.doi.org/10.1016/j.physe.2017.08.013>.
13. P. Ballet, J. B. Smathers, H. Yang, C. L. Workman, and G. J. Salamo, Control of size and density of InAs/(AlGa)As self-organized islands. *Journal of Applied Physics* **481** (2001). <https://doi.org/10.1063/1.1357784>.
14. T.J. Krzyzewski, P. B. Joyce, G. R. Bell, T. S. Jones. Understanding the growth mode transition in InAs/GaAs (001) quantum dot formation. *Surface Science*, (2003) 532. [https://doi.org/10.1016/S0039-6028\(03\)0045-2](https://doi.org/10.1016/S0039-6028(03)0045-2).
15. H. T. Dobbs, D.D. Vvedensky, A. Zangwill, J. Johansson, N. Carlsson, W. Seifert. Mean-Field Theory of Quantum Dot For-

- mation. *Phys. Rev. Lett.* **79** (1997) 897, <https://doi.org/10.1103/PhysRevLett.79.897>.
16. C. Priester. Modified two-dimensional to three-dimensional growth transition process in multistacked self-organized quantum dots. *Phys. Rev. B.* **153303** (2001) 1, <https://doi.org/10.1103/PhysRevB.63.153303>.
 17. C. A. Mercado-Ornelas, L. I. Espinosa-Vega, I. E. Cortes-Mestizo, F. E. Perea-Parrales, A. Belio-Manzano, and V. H. Mendez-Garcia. Nucleation and diffusion processes during the stacking of bilayer quantum dot InAs/GaAs heterostructures. *Journal of Crystal Growth*, **555** (2021) 0022, <https://doi.org/10.1016/j.jcrysgro.2020.125959>.
 18. H. Z. Song, T. Usuki, Y. Nakata, N. Yokoyama, H. Sasakura, and S. Muto, Formation of InAsGaAs quantum dots from a subcritical InAs wetting layer: A reflection high-energy electron diffraction and theoretical study. *Physical Review B*, **73** (2006) 115327, <http://dx.doi.org/10.1103/PhysRevB.73.115327>.
 19. C.A. Mercado-Ornelas *et al.*, *Physica E: Low-dimensional Systems and Nanostructures* **114217** (2020) 1386, <https://doi.org/10.1016/j.physe.2020.114217>.
 20. D. Panda *et al.*, Optimization of dot layer periodicity through analysis of strain and electronic profile in vertically stacked InAs/GaAs Quantum dot heterostructure. *Journal of Alloys and Compounds*, **0925-8388** (2018) 216, <https://doi.org/10.1016/j.jallcom.2017.11.086>.
 21. Y. Xiong, and X. Zhang. InAs/InP quantum dots stacking: Impact of spacer layer on optical properties *J. Appl. Phys.* **093103** (2019), <https://doi.org/10.1063/1.5082722>.
 22. P. B. Joyce, T. J. Krzyzewski, P. H. Steans, G. R. Bell, J. H. Neave, and T. S. Jones, Shape and surface morphology changes during the initial stages of encapsulation of InAs/GaAs quantum dots. *Surface Science* **492** (2001) 345, [https://doi.org/10.1016/S0039-6028\(01\)01479-0](https://doi.org/10.1016/S0039-6028(01)01479-0).
 23. A. Hospodkova, J. Vyskocil, J. Pangrac, J. Oswald, E. Huličius, and K. Kuldova, *Surface Science*, **604** (2010) 3, <https://doi.org/10.1016/j.susc.2009.11.023>.
 24. H. Z. Song, Y. Tanaka, T. Yamamoto, N. Yokoyama, M. Sugawara, and Y. Arakawa, Surface processes during growth of InAs/GaAs quantum dot structures monitored by reflectance anisotropy spectroscopy. *Physics Letters A*, **375** (2011) 3517, <https://doi.org/10.1016/j.physleta.2011.08.021>.
 25. E. C. Weiner *et al.*, Effect of capping procedure on quantum dot morphology: Implications on optical properties and efficiency of InAs/GaAs quantum dot solar cells. *Solar Energy Materials and Solar Cells*, **178** (2018) 240, <https://doi.org/10.1016/j.solmat.2018.01.028>.
 26. B. Tongbram, J. Saha, S. Sengupta and S. Chakrabarti, Metamorphosis of self-assembled InAs quantum dot through variation of growth rates. *Journal of Alloys and Compounds* **153870** (2020) 824 <https://doi.org/10.1016/j.jallcom.2020.153870>.
 27. A. Taurino *et al.*, InAs/AlGaAs quantum dots grown by a novel molecular beam epitaxy multistep design for intermediate band solar cells: physical insight into the structure, composition, strain and optical properties. *Cryst. Eng. Comm.*, **21** (2019) 4644, <https://doi.org/10.1039/C9CE00792J>.
 28. P. Howe, E. C. Le Ru, R. Murray, T. S. Jones. Indium segregation during multilayer InAs/GaAs(0 0 1) quantum dot formation. *Journal of Crystal Growth*, **278** (2005) 57, <http://dx.doi.org/10.1016/j.jcrysgro.2004.12.053>.
 29. K. B. Hong and M. Kuo, Proceedings of the ASME 2009 International Mechanical Engineering Congress and Exposition (IMECE2009). Effects of segregation on the strain fields and electronic structures of the InAs quantum dots. (2009) <https://doi.org/10.1115/IMECE2009-11917>.
 30. S. Adhikary *et al.*, Investigation of strain in self-assembled multilayer InAs/GaAs quantum dot heterostructures. *Journal of Crystal Growth*, **3012** (2010) 724, <https://doi.org/10.1016/j.jcrysgro.2009.11.067>.
 31. Y. I. Mazur, Zh. M. Wang, and G. J. Salamo, Investigation of indium distribution in InGaAs/GaAs quantum dot stacks using high-resolution x-ray diffraction and Raman Scattering. *Journal of Applied Physics* **023517** (2006) 99, <http://dx.doi.org/10.1063/1.2163009>.
 32. G. Polupan, T. Torchynska, L. G. Vega Macotela, R. Cisneros Tamayo and A. Escobosa Echavarrá. Emission and HR-XRD varying in GaAs/AlGaInAs heterostructures with InAs quantum dots at annealing. *J. Mater. Sci: Mater Electron*, **31** (2020) 2643, <https://doi.org/10.1007/s10854-019-02803-x>.
 33. T. Sugaya *et al.*, Ultra-high stacks of InGaAs/GaAs quantum dots for high efficiency solar cells. *Energy Environ. Sci.* **5** (2012) 6233, <https://doi.org/10.1039/C2EE01930B>.
 34. M. Souaf *et al.*, Investigation of the InAs/GaAs Quantum Dots Size: Dependence on the Strain Reducing Layers Position. *Materials*, **8** (2015) 4699, <https://doi.org/10.3390/ma8084699>.
 35. L. Seravalli, M. Minelli, P. Frigeri, and S. Franchi, Quantum dot strain engineering of InAs/InGaAs nanostructures. *Journal of Applied Physics* **101** (2007) 024313, <https://doi.org/10.1063/1.2424523>.
 36. R. Songmuang, S. Kiravittaya and O. G. Schmidt, Shape evolution of InAs quantum dots during overgrowth. *Journal of Crystal Growth*, **249** (2003) 416, [https://doi.org/10.1016/S0022-0248\(02\)02222-4](https://doi.org/10.1016/S0022-0248(02)02222-4).
 37. M. Schramboeck *et al.*, InAs/AlGaAs QDs for inter-subband devices. *Superlattices and Microstructures*, **44** (2008) 0749, <https://doi.org/10.1016/j.spmi.2007.10.010>.
 38. Y. Li, Vertical coupling effects and transition energies in multilayer InAs/GaAs quantum dots. *Surface Science* **039-6028** (2004) 566. <https://doi.org/10.1016/j.susc.2004.06.052>.
 39. C. Shu and Y. Liu, The Calculation for Strain Distributions and Electronic Structure of InAs/GaAs Quantum Dots Based on the Eight-Band k.p *Theory Acta Physica Polonica. A.* **3** (2016) 371, <http://doi.org/10.12693/APhysPolA.129.371>.